**Self-Archived version:**

Campione A, Cipollina A, Bogle IDL, Gurreri L, Tamburini A, Tedesco M, et al. A hierarchical model for novel schemes of electrodialysis desalination. Desalination 2019;465:79–93. doi:10.1016/j.desal.2019.04.020.

# *A hierarchical model for novel schemes of electrodialysis desalination*

*A. Campione[a], A. Cipollina[a,*], I. D. L. Bogle[b], L. Gurreri[a], A. Tamburini[a], M. Tedesco[c], G. Micale[a]*

[a]*Dipartimento di Ingegneria, Università degli Studi di Palermo, viale delle Scienze Ed.6, 90128 Palermo, Italy*

[b]*Centre for Process Systems Engineering, Department of Chemical Engineering, University College London, Torrington Place, London WC1E 7JE, UK.*

[c]*Wetsus, European Centre of Excellence for Sustainable Water Technology, Oostergoweg 9, 8911 MA Leeuwarden, The Netherlands*

[*]*Corresponding Author (A. Cipollina):* andrea.cipollina@unipa.it

*Abstract*

A new hierarchical model for the electrodialysis (ED) process is presented. The model has been implemented into *gPROMs Modelbuilder (PSE)*, allowing the development of a distributed-parameters simulation tool that combines the effectiveness of a semi-empirical modelling approach to the flexibility of a layered arrangement of modelling scales. Thanks to its structure, the tool makes possible the simulation of many different and complex layouts, requiring only membrane properties as input parameters (e.g. membrane resistance or salt and water permeability). The model has been validated against original experimental data obtained from a lab scale ED test rig. Simulation results concerning a 4-stage treatment of seawater and dynamic batch operations of brackish water desalination are presented, showing how the model can be effectively used for predictive purposes and for providing useful insights on design and optimisation.

***Keywords:*** *Multi-scale model; simulation; multistage; ion exchange membrane; electromembrane process.*

## 1. Introduction

It has been estimated that two thirds of the world's population currently experience water scarcity for at least one month a year [1]. Despite this, the global water demand is expected to grow year by year. Nowadays, agriculture is responsible for 70% of water consumption, although the increase of demand will also be caused by industry and energy production needs [1]. In this context, water desalination might have a crucial role, and a wide range of technologies has been developed in the last decades [2]. In fact, almost 100$Mm^3$/day of cumulative contracted capacity has been reported for the year 2016 [3], and such capacity is expected to steadily increase during the next decades.

Generally, desalination technologies can be classified into thermal and membrane processes. The first group is mainly constituted by multistage flash (MSF) and multi effect distillation (MED), while reverse osmosis (RO) and electrodialysis (ED) are the main membrane processes [2]. Thermal processes have represented the industrial standard for many years. However, nowadays they occupy approximately 34% of the world desalination capacity while RO accounts for the 60% on its own [4,5]. On the other hand, ED has a much smaller market share and has been mainly used for brackish water desalination [6].

ED is an electro-membrane process, which comprises a series of anion and cation exchange membranes (AEMs, CEMs) arranged alternatively and separating the fluid channels between two electrodic compartments (Figure 1). When the electrodes are connected to a source of electric potential, an ionic current is driven through the assembly where the solution to be desalted flows along the channels created in the space in between two membranes. Therefore, anions in solution migrate towards the anode (positively charged) and cations towards the cathode (negatively charged).

Consequently, the series of CEMs and AEMs allows the selective separation of ions and thus the creation of concentrated and diluted solutions inside channels. An AEM, a CEM and two adjacent channels compose the cell pair, i.e. the ED repeating unit. The number of cell pairs inside a single unit (stack) ranges from a few pairs (laboratory scale) up to several hundred (industrial scale) [7]. Channels are usually created by the presence of net spacers, provided with gaskets, separating adjacent membranes and driving the fluid motion along different possible patterns depending on the spacer shape. The net spacer geometry plays also a significant role in the mixing promotion [6,7]. Recently, the possibility of using profiled membranes in spacer-less stacks has also been assessed [6–8].

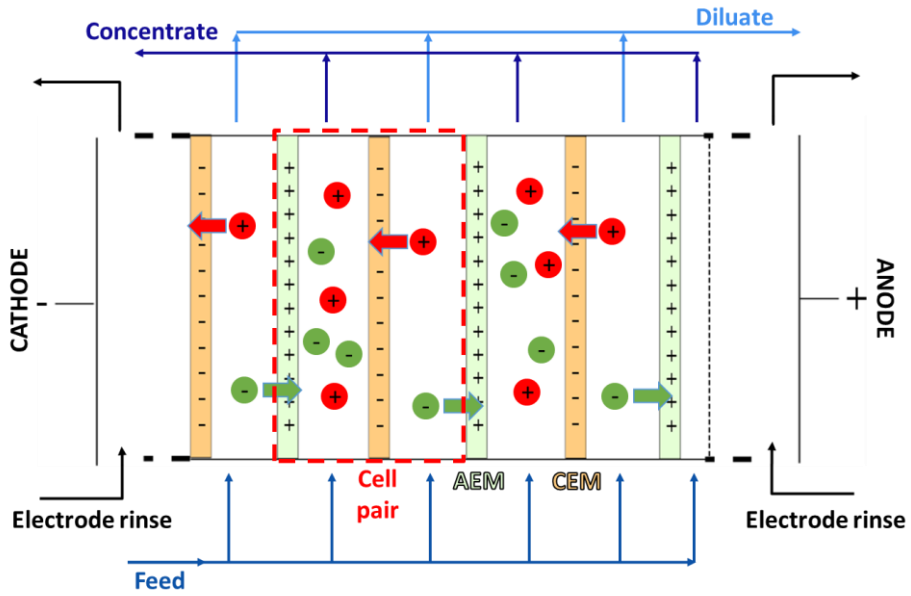


*Figure 1. Scheme of the ED process.*

Over the years, ED has been applied for different purposes. Whey demineralisation, tartrate acid stabilisation in wine and fruit juice de-acidification represent some examples in food industry [9–11]. The ED process has also been widely used for production of organic acids [12] and for wastewater treatment, especially for heavy metal removal [13–15]. Another important ED application is the production of table salt , especially in Japan with about 1 million ton per year of production capacity

[6,16]. Despite all these different applications, water desalination is the main industrial application field. ED plants currently installed all over the world have production capacities ranging between 2 and 145,000 $m^3$/day [17]. In particular, ED demonstrated its competitiveness with low-concentration feeds (< 2500 ppm) showing comparable performance with RO units [17–20].

Although its conceptualization is relatively far back in time [21,22], it is worth noting how the use of ED for water desalination has been being gradually gaining attention in the last years. As a matter of fact, the actual trend is pushing towards ion-exchange membranes (IEMs) development [23] and cost reduction [24]. Another two interesting development areas are represented by the coupling of ED with off-grid energy sources [25,26] or with salinity gradient power/osmotic dilution devices [24,27,28], with the latter that could be applied in seawater desalination. With respect to these aspects, the EU-funded project *REvivED Water* [24] is worth mentioning for its focus on the assessment of commercialisation of some of these new ideas, including brackish water ED with capacitive electrodes, multistage ED for seawater desalination and coupling of ED with reverse electrodialysis (RED) and/or RO.

All of these new developments strongly require the support of modelling activities as they introduce further complications compared to the standard ED such as the need for dynamic simulations, multivariable optimisation and/or articulated combinations of processes.

## 2. Overview of modelling approaches for electrodialysis

During the last years, a number of ED models have been proposed based on different approaches [7]. The first category includes all the **simplified models**, which are usually developed with the aim of performing preliminary design [29] or to study a very specific system relying on experimentally fitted parameters [30]. In this case, several assumptions are generally used and lumped parameters are

considered. Typically, overall quantities, such as the required membrane area to perform a certain desalination or the total power consumption, can be estimated.

The second category is represented by the **advanced models**, which, differently from the previous ones, take into account several phenomena causing deviations from the ideal behaviour. Advanced models can be sub-classified in theoretical and semi-empirical.

**Theoretical models** for (reverse) electrodialysis are based on the solution of rigorous equations (i.e. Nernst-Planck [31–37], or even the more complex Stefan-Maxwell equations [38–40]) that mathematically describe local transport phenomena. However, these models require a number of thermodynamic and electrochemical parameters that cannot always be easily determined. In addition, the large amount of computational power required to solve this kind of models makes them suitable only for simplified geometries [7].

**Semi-empirical models** for (reverse) electrodialysis are based on the use of mass balances and detailed transport equations accounting for salt and water fluxes through the membranes and on the calculation of the voltage drop by the segmentation approach (cell pair simulated as a multi-layer that, in the most complete models, includes the diffusion boundary layers). They require (i) empirical information such as membrane properties, being available from manufacturers or easily measured by experiments (transport numbers, ohmic resistance, salt permeability, osmotic permeability, etc.), and (ii) a lower computational power. These features make this modelling approach suitable for faster and more reliable predictions than the theoretical models, especially in the simulation of realistic geometries of channels and stacks, which are more complicated than the simplified configurations typically assumed in theoretical models [7]. Semi-empirical models can be based on lumped parameters [41–48]. However, in this case they have limited prediction capabilities, providing accurate results only under some conditions [47]. On the contrary, distributed parameters models [49–56] are more accurate, but at the cost of a larger implementation effort. In summary, with respect to

the theoretical models, 1-D semi-empirical models are preferable as process simulators thanks to their features of versatility, robustness and effectiveness.

Some advanced semi-empirical models use a "practical" current density calculated as a fraction of an experimentally determined limiting current density [45–47]. Many other models of this category, instead, adopt a multi-scale approach treating the lower scale mass transfer phenomena (Sherwood number and, thus, concentration polarization) for calculating the voltage drop with different approaches. In particular, the majority makes use of either empirical information [42–44,48,52,55,57] (e.g. limiting current density) or 3-D computational fluid dynamics (CFD) simulations [50,51,54,56]. Numerical simulations can also predict pressure drops and ohmic resistance [50].

In the model recently proposed by Chehayeb and co-workers [41,49,53] the diffusion boundary layer thickness was calculated by experimental data on the Sherwood number, while mass transport in the boundary layer was simulated by the Maxwell-Stefan approach in order to predict concentration and electrical potential profiles and ionic and water fluxes. In ref [53] three different applications were simulated: brackish water desalination (from 3 to 0.35 g/kg), partial seawater desalination (from 35 to 1 g/kg) and brine concentration (from 70 to 200 g/kg). Moreover, two-stage operations were shown to be effective in energy saving.

Wright et al. [55] proposed a semi-empirical model of ED for brackish water desalination, then used for a cost analysis for domestic applications of groundwater treatment [57]. A sensitivity analysis accompanied by a comparison with experimental data on ED units operated in batch mode showed that a number of simplifying assumptions (such as ideal permselectivity, negligible water transport, and constant membrane resistance) are certainly acceptable when using the model under "conventional" operations and low feed concentrations (up to 3.5 g/l). However, in the case of high salinity feed solutions (e.g. seawater or concentrated brine) such assumptions are not valid and would lead to erroneous predictions.

On one hand, the number of recently published works shows the current significant interest of the scientific community in the development of effective and reliable modelling tools for (reverse) electrodialysis. On the other hand, however, 1-D process simulators have been poorly devoted to study non-conventional ED applications, such as seawater desalination and multistage configurations. In this study, we propose a 1-D semi-empirical hierarchical model of the ED process, based on a robust and generalised approach developed for a wide range of operating conditions (from brackish to sea water feed solutions), and of any scale of application, spanning from bench stacks to industrial plants, and for both single and multistage configurations. The model takes into account the main phenomena involved in determining the process performance, with the aim to achieve reliable simulation results in different scenarios, thus providing a useful tool for process design and optimization. The model was validated against experimental data, and was used to study some applications poorly explored so far, focusing on a 4-stage system of seawater desalination and on single-stage batch operations of brackish water desalination.

## 3. Modelling

The process model is based on a hierarchical semi-empirical approach, schematically represented in Figure 2. The lowest scale is represented by the cell pair (I), the repeating unit of an ED unit composed by an AEM, a CEM and two adjacent channels. The higher scale of the stack (II) is modelled by considering a series of cell pairs and the electrodes. Finally, the stack model can be used in the highest scale of the overall plant (III), where the stacks can be variously arranged, thus simulating different process layouts (i.e. single stage, multistage, batch, feed and bleed etc.).

A number of assumptions characterises the model, in particular:

- A one-dimensional approach is adopted, in order to simulate distribution profiles along the channels, thus co- and counter-current arrangements can be simulated, while changes along the direction of the channel width are neglected:
- The presence of salt other than NaCl is neglected, thus a single salt solution is simulated;
- The unit operates below the limiting current;
- The effect of parasitic currents *via* manifolds is not taken into account;
- Transport numbers inside IEMs (and thus membrane permselectivity) are assumed independent of salt concentration in the solutions;
- The flow distribution is homogeneous among all cell pairs.

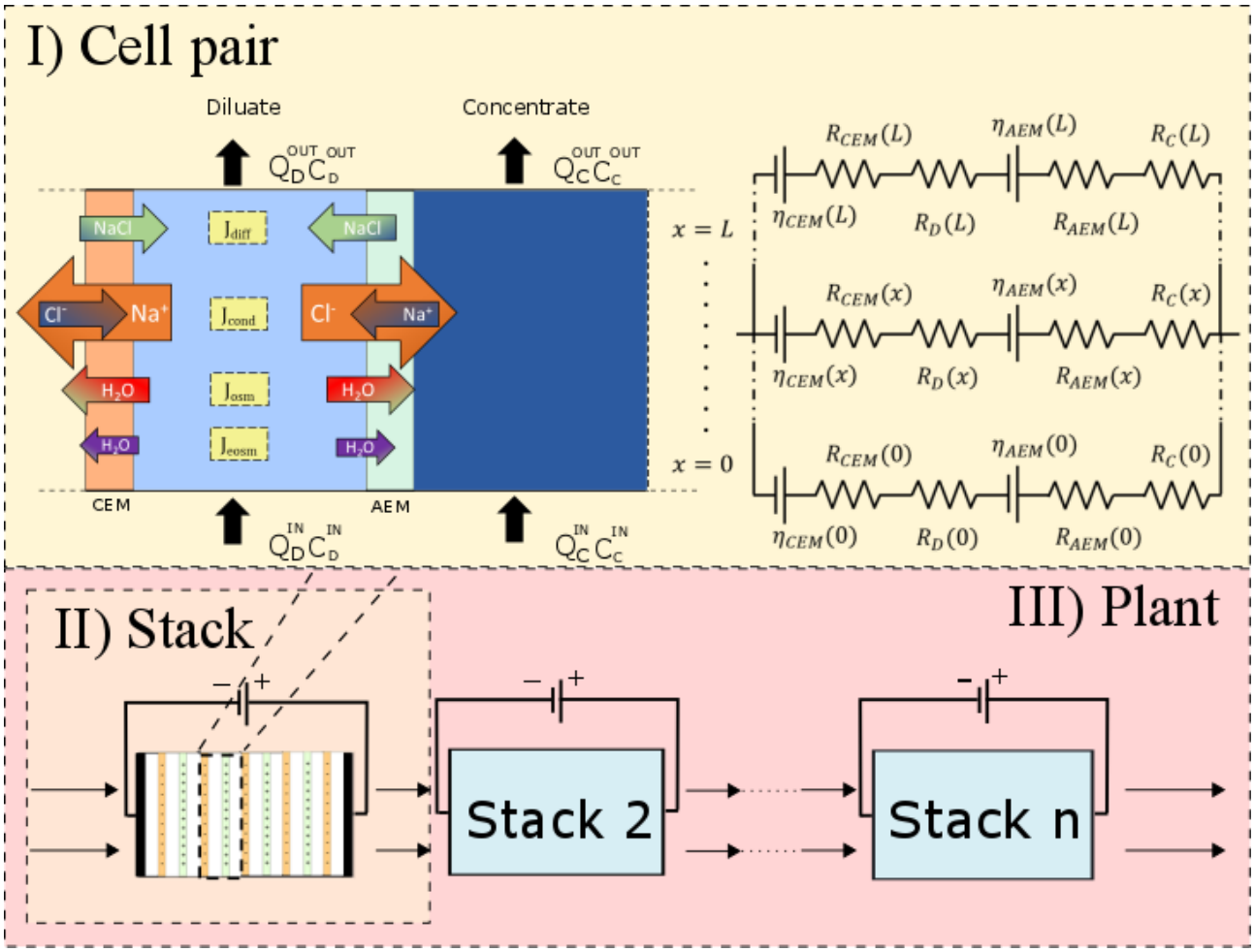


*Figure 2. Schematic description of the hierarchical approach showing I) Cell pair, with the main transport mechanisms, II) Stack, III) Overall plant (i.e. multistage system).*

## 3.1 Cell pair

At the scale of the cell pair (Figure 2 I), mass balances, transport phenomena, solutions thermodynamics and electrical parameters are described.

### *3.1.1 Transport phenomena and mass balance*

Different transport phenomena take place inside the cell pair, causing both salt and water to move through membranes. The main salt transport mechanism is the conductive flux, which is proportional to the generated ionic current and is associated to the external applied voltage. In a general position along the length of the cell pair, it can be calculated as:

$$J_{cond}(x) = [t_{CEM}^{counter} - (1 - t_{AEM}^{counter})] \frac{i(x)}{F} \quad (1)$$

where $i$ is the current density, $F$ is the Faraday constant, and $t_{CEM}^{counter}$ and $t_{AEM}^{counter}$ are the transport numbers of the counter-ions inside the IEMs, directly linked with the membrane permselectivity (see Appendix A). In addition to the effects on the conductive flux, another consequence of the non-perfect membrane selectivity is the occurrence of a back-diffusive salt flux driven by the salt concentration difference between the channels, which, for a single membrane, can be written as:

$$J_{diff}^{IEM}(x) = -\frac{D^{IEM}}{\delta^{IEM}}(C_C{}^{int,IEM}(x) - C_D{}^{int,IEM}(x)) \quad (2)$$

where $D$ is the salt permeability coefficient through the IEMs, $\delta$ is the thickness of IEMs and $C^{int}$ is the salt concentration in solution at the interface with the membrane. Subscripts $C$ and $D$ refer to concentrate and diluate respectively and the superscript $IEM$ indicates that, using the relevant values, the expression is valid for both AEM and CEM. The overall diffusive flux can be written as the sum of the fluxes through the two membranes.

Also water molecules can move through the membranes. Water transport can be attributed to two phenomena: osmosis and electroosmosis. The first transport mechanism is caused by the interfacial concentration gradient between concentrate and diluate and can be expressed as:

$$q_{osm}^{IEM}(x) = L_p^{IEM}(\pi_C^{IEM} - \pi_D^{IEM}) = L_p^{IEM}\left[\nu R_G T\left(\varphi_C^{IEM} C_C{}^{int,IEM}(x) - \varphi_C^{IEM} C_D{}^{int,IEM}(x)\right)\right] \quad (3)$$

where $L_p$ is the water permeability coefficient of IEMs and $\pi$ is the osmotic pressure that can be related to the van 't Hoff coefficient ($\nu$), the osmotic coefficient ($\varphi$) and the solution concentration. Pitzer's correlation is used to estimate osmotic coefficients [58,59], as described in Appendix B. As for the diffusive flux, the total osmotic flux is the sum of the fluxes on the two membranes.

The second transport mechanism, electroosmosis, is the water flux coupled with the ions movement due to two main contributions: the water molecules of the solvation shell and the water flux dragged by the momentum arising on the slip-plane between the solvation shell and the solvent [60,61]. Generally, electroosmosis can be expressed as a function of the overall salt flux:

$$q_{eosm}(x,t) = \frac{w\, J_{tot}(x,t) M_w}{\rho_w} \quad (4)$$

where $J_{tot}(x)$ is the sum of the diffusive (of both AEM and CEM) and the migrative salt flux and $w$ is the total water transport number, defined as the sum of the water transport number relative to each ion. In [60], Wilson reports that for most membranes the ionic transport numbers are close to the primary hydration numbers. Thus, for a NaCl solution a value of 12 moles per equivalent of transported salt can be assumed.

The model computes distributions over the dimension of the channel length. Bulk concentration and flowrate distributions inside the channels are described through differential mass balance equations that, in the case of co-current flow and negligible changes in the solutions density, are:

$$\frac{d\, Q_D(x)\, C_D(x)}{dx} = -b\, J_{tot}(x) \quad (5) \qquad \frac{d\, Q_C(x)\, C_C(x)}{dx} = b\, J_{tot}(x) \quad (6)$$

$$\frac{d\,Q_D(x)}{dx} = -\,b\,q_w(x) \qquad (7) \qquad\qquad \frac{d\,Q_C(x)}{dx} = \;b\,q_w(x) \qquad (8)$$

where $Q(x)$ represents the local volumetric flow rate, $b$ the channel width and $q_w(x)$ the local overall volumetric water flux (i.e. the sum of osmotic and electroosmotic fluxes).

### *3.1.2 Electric variables, concentration polarization and pressure drops*

A crucial aspect of ED process modelling is to relate the ionic current to the applied voltage. The voltage drop over a cell pair ($\Delta V_{cp}$) is calculated as:

$$\Delta V_{cp} = \eta\,(x) + R_{tot}(x)i(x) \qquad (9)$$

where $\eta$ is the non-ohmic voltage drop associated to the back electromotive force (diffusion potentials are not taken into account), $i$ is the current density, $R_{tot}$ is the total areal ohmic resistance of cell pair that can be calculated as the sum of the four components in series

$$R_{tot}(x) = R_{CEM}(x) + R_{AEM}(x) + R_C(x) + R_D(x) \qquad (10)$$

where $R_{CEM}$ and $R_{AEM}$ represents the resistance of IEMs. $R_C$ and $R_D$ are the resistance of concentrate and diluate respectively, and, neglecting the ohmic contribution of the diffusion boundary layers, can be generally expressed as:

$$R_{SOL}(x) = f_{s_{SOL}}\,\frac{\delta_{SOL}}{\Lambda_{SOL}(x)\,C_{SOL}(x)} \qquad (11)$$

with $\delta$ being the compartment thickness, $f_s$ the shadow factor, which accounts for the resistance increase due to the presence of a non-conductive spacer [51] and $\Lambda$ the equivalent conductivity. The subscript $SOL$ refers to the generic solution, thus making the equation valid for both concentrate and diluate resistances by using the relevant parameters. For a NaCl salt solution, the equivalent conductivity can be estimated by the correlation of Islam et al. [62], as described in Appendix C. The shadow factor is generally a function of the geometrical characteristics of the spacer. Therefore, it is usually calculated as a function of the channel porosity [52,54], open area [51], or both [63,64]. The

porosity represents the fraction of channel volume occupied by the liquid, while the open area represents the free fraction of membrane area projected in the direction perpendicular to membranes. Values for the open area typically range between 40-60% [51]. In this study, the shadow factor for the simulated spacer has been calculated by finite-volume simulations (solving the Laplace equation for the electric potential), resulting in a value that is close to the reciprocal of the average of porosity and open area, and is in agreement with experimental findings [65].

It is known that membrane resistance is influenced by solution concentration [66–68]. In particular, it has been shown that dilute concentration has the biggest effect. The effect of concentration on IEMs has been taken into account in the model, following the relationship from Galama et al. [66]. More details can be found in Appendix D.

The non-ohmic contribution of the voltage drop ($\eta$) is the sum of the membrane potentials that are established within all cell pairs due to the different salt concentration between flowing solutions. A simplified expression of the membrane potential can be derived from the Teorell-Meyer-Sievers theory [69,70]. Taking also into account concentration polarisation effects, the non-ohmic drop can be calculated as follows:

$$\eta(x) = \eta_{CEM}(x) + \eta_{AEM}(x) \tag{12}$$

$$\eta_{IEM}(x) = \alpha_{IEM} \frac{R_G T}{F} ln\left[\frac{\gamma_C^{int,IEM}(x)\, C_C^{int,IEM}}{\gamma_D^{int,IEM}(x)\, C_D^{int,IEM}}\right] \tag{13}$$

where $\alpha_{IEM}$ is the permselectivity of one IEM, $\gamma^{int}$ and $C^{int}$ represent the activity coefficient and the salt concentration, respectively, at the membrane-solution interface. Activity coefficients are estimated through the Pitzer's correlation [58,59] (see Appendix B).

The salt concentrations at the solution-membrane interfaces are estimated as functions of the current density and the Sherwood number, the latter being calculated by CFD correlations (see Appendix E).

## 3.2 Stack

### *3.2.1 Electrical model*

At the higher hierarchy level, overall quantities are estimated and the voltage drop within the electrode compartments is taken into account. Therefore, the overall voltage applied to the stack is calculated as:

$$V_{tot} = \frac{R_{blank} I}{A} + \sum_{i=1}^{N_{cp}} \Delta V_{cp_i} \tag{14}$$

where $V_{tot}$ is the overall applied voltage, $A$ is the area of a single membrane, $R_{blank}$ is the blank resistance, accounting for electrode compartments, $I$ is the overall current, calculated as the integral of the current density over the active area, and $N_{cp}$ is the number of cell pairs in the stack.

### *3.2.2 Energy consumption, current efficiency, apparent flux*

In the stack model, most of the energetic parameters are also computed. The total power required to desalinate a certain amount of water is the sum of the electric energy supplied to the stack, plus the energy needed for pumping the solutions. The total power consumption is:

$$P = V_{tot}\, I \; + \; \Delta p_C^{tot} Q_D^{av} + \; \Delta p_C^{tot} Q_D^{av} \tag{15}$$

where $Q^{av}$ is the average solution flowrate and $\Delta p^{tot}$ is the overall pressure drop through the stack, i.e. including hydraulic losses in the manifolds and in the channels (Appendix E).

In addition, the energy consumption per unit volume of product (here represented by the diluate) can be defined as:

$$E_{spec} = \frac{P}{Q_D^{OUT,tot}} \tag{16}$$

where $Q_D^{OUT,tot}$ is the overall outlet diluate flowrate and $E_{spec}$ is the specific energy consumption expressed in kWh/m$^3$. Moreover, the salt-specific energy consumption can be defined as:

$$E_{spec}^{salt} = \frac{P}{C_D^{IN} Q_D^{IN,tot} - C_D^{OUT} Q_D^{OUT,tot}} = \frac{P}{C_C^{OUT} Q_C^{OUT,tot} - C_C^{IN} Q_C^{IN,tot}} \quad (17)$$

where superscripts *IN* and *OUT* refer to inlet and outlet conditions. Eq. (17) is particularly useful when the separation target is related to salt removal rather than to the volume of diluate produced.

Other two figures of merit have been defined to analyse the process performance. The first one is the current efficiency, which can be expressed as:

$$\xi = \frac{(C_D^{IN} Q_D^{IN,tot} - C_D^{OUT} Q_D^{OUT,tot}) \cdot F}{I \cdot N_{cp}} \quad (18)$$

The current efficiency represents the amount of current that is actually converted into useful salt flux, thus expressing the efficiency of current utilisation of the process [60] .

The second parameter is the apparent product flux (or water productivity [20]) and it is defined as:

$$J_P = \frac{Q_D^{OUT,tot}}{2A\, N_{cp}} \quad (19)$$

This variable gives an indication of the area required to obtain a certain flowrate of desalinated water. This is very useful for comparison with other desalination processes such as reverse osmosis, where the flux is often used as performance indicator.

### 3.3 Overall plant

The main advantage of using a hierarchical approach is that the stack model can be inserted into higher hierarchy models in order to simulate complex plant layouts. In this work, multistage and batch operations have been analysed as examples of articulated flowsheeting.

### *3.3.1 Multistage ED*

A multistage configuration requires a number of stacks that can be connected according to different schemes, some of which are reported as example schemes in Appendix F. As case study, a multistage operation in series can be arranged with either a co-current or a counter-current scheme (Figure 8).

In a multistage system, it is more convenient to define the specific energy consumption of the overall system as follows:

$$E_{spec}^{TOT} = \frac{\sum_{i=1}^{N_s} P_i}{Q_{D,N_s}^{OUT,tot}} \tag{20}$$

where $N_s$ is the number of stages and $Q_{D,N_s}^{OUT,tot}$ is the diluate flowrate coming out from the last stack.

In the same way, the water productivity for the overall system will contain the diluate flowrate coming out from the last stack

$$J_P = \frac{Q_{D,N_s}^{OUT,tot}}{\sum_{i=1}^{N_s} N_{cp,i}\, 2A_i} \tag{21}$$

Generally, a multistage system has the advantage to reduce the energy requirements of a certain desalination operation compared to a single stage operating at the same conditions. On the other hand, the system design and optimisation complexity increases with the number of stages, as it becomes necessary to deal with more variables. Therefore, it becomes crucial to support such design operations with simulations. A common issue can be the optimisation of the applied voltage per each stage in order to minimise the energy consumption. In addition, it is also possible to test the stages with more complex arrangements that may include recycles or splitting of the streams.

### *3.3.2 Batch ED*

The model can also deal with the simulation of transient operations of batch ED systems (the example scheme is reported in Figure 9 of Appendix F). In this case, an additional model of lower hierarchy

describing the tanks is defined, thus predicting the time variation of solutions concentration and volume within the tanks. Assuming that the tanks are perfectly mixed, this model is characterised by the following time dependent differential equations:

$$\frac{d(V_{tank} \cdot C_{tank})}{dt} = Q_{tank}^{IN} C_{tank}^{IN}(t) - Q_{tank}^{OUT} C_{tank}(t) \quad (22)$$

$$\frac{dV_{tank}}{dt} = Q_{INtank}^{IN}(t) - Q_{tank}^{OUT}(t) \quad (23)$$

where $V_{tank}$ is the solution volume inside the tank, $C_{tank}$ is the salt concentration in the solution inside the tank (i.e. entering the stack), $Q_{tank}^{IN}$ and $C_{tank}^{IN}$ are the flowrate and salt concentration of the solution going into the tank (i.e. coming out from the stack) and $Q_{tank}^{OUT}$ is the solution flowrate exiting the circulation tank. In addition, two initial conditions are required for volume and concentration. Using the relevant initial conditions, the aforementioned model is indistinctly applicable to the diluate and concentrate tanks. Assuming that stack dynamics is negligible compared to the time variation of concentrations in the tanks, a quasi-steady state approach can be adopted to combine the dynamic tank model to the steady state ED stack model.

## 4. Experimental

An experimental campaign was carried out in order to validate the model. All the experiments were conducted in a single ED stack (*Deukum GmbH*, Germany). The ED unit was equipped with 10 cell pairs, with an active membrane area of 10×79 $cm^2$ and woven spacers 270 µm thick (*Deukum GmbH, Germany*). Homogeneous ion exchange membranes (*FUJIFILM Manufacturing Europe B.V., The Netherlands*) were used for all the tests. The relevant properties of both AEMs and CEMs (as provided by the membrane manufacturer) are reported in Table 1. The electrodialysis tests were performed under galvanostatic mode, using a power supply (*Elektro-Automatic GmbH, Germany).*

*Table 1. Properties of the Fujifilm membranes (provided by the manufacturer).*

| Membrane | Thickness δ (μm) | Permselectivity α* | Water permeability $L_p$ (ml/(bar h $m^2$)) | Resistance R (Ω $cm^2$)** |
|---|---|---|---|---|
| **AEM** | 130 | 0.969 | 6.29 | 1.77 |
| **CEM** | 130 | 0.975 | 7.79 | 1.89 |

*Permselectivity measured in between 0.05M/0.5M KCl solutions

**Membrane resistance measured with 0.5 M NaCl solution

Artificial salt water at different concentrations was prepared by using re-crystallised NaCl with purity >99.5% (*Saline di Volterra s.r.l.*, Italy), and demineralized water. The electrode rinse solution was a 10 g/l $Na_2SO_4$ aqueous solution, operating at 700 ml/min. Feed and electrode rinse solutions were pumped by three peristaltic pumps (*Lead Fluid Technology Co., Ltd., China*). Single pass experiments were performed. Conductivity measurements were performed at the concentrate and diluate outlets by conductivity meters (*XS instruments, Italy*), while glycerin-filled pressure gauges (*Cewal S.p.a., Italy*) were placed at the inlets to measure pressure drops.

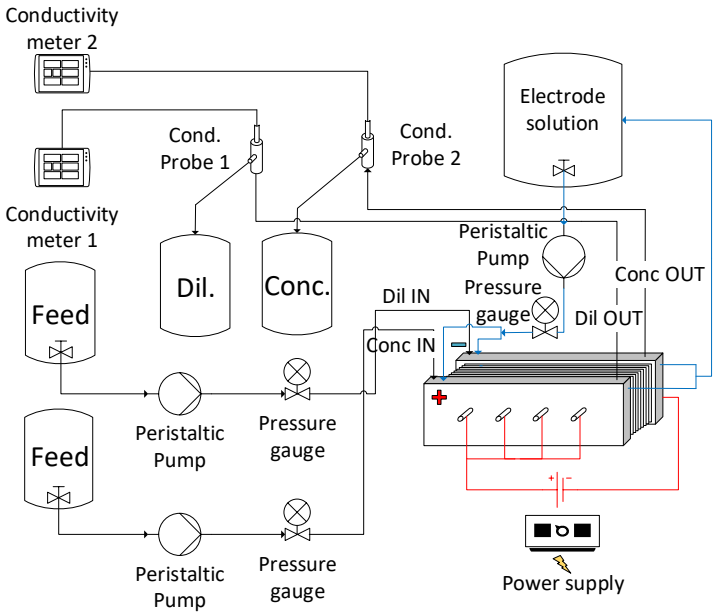


*Figure 3. Schematic representation of the experimental set-up.*

A schematic representation of the set-up is presented in Figure 3. For every experiment, the stack was operated with feed water (at the given flowrate and concentration) for at least 5 minutes, to ensure proper membrane conditioning and steady state conditions. Then, a constant current was applied, until a stable value of the outlet conductivity was reached. A summary of the main process conditions (i.e., inlet concentrations, velocities, and currents) is given in Table 2.

*Table 2. Summary of the main process conditions of the experimental tests.*

| $C^{IN}$ (g/l) | u (m/s) | I (A) | $i_{av}$ (A/m$^2$) |
|---|---|---|---|
| **1** | 0.7-2.5 | 0.2-0.5 | 2.5 - 6.25 |
| **3** | 0.7-2.5 | 0.2-1.5 | 2.5 - 18.75 |
| **6** | 0.5-2.2 | 0.2-4 | 2.5 - 50 |
| **10** | 0.5-2.25 | 0.2-7 | 2.5 - 87.5 |
| **30** | 0.45-2.25 | 0.2-10 | 2.5 - 125 |

## 5. Results and discussion

In this section, the model is validated against original experimental data. Then, the model predictions for two representative cases (i.e. multistage ED for seawater and single-stage batch ED for brackish water) are presented and discussed.

### 5.1 Model validation for brackish water and seawater conditions

Model predictions were compared with experimental results over a wide range of inlet concentrations (i.e. from 1 to 30 g/l), electrical currents and flow velocities. A representative part of the experimental points is depicted in Figure 4, reporting the comparison between model predictions and experimental values of outlet conductivities for both concentrate and diluate. Model results fit very well

experimental data of conductivities as functions of the current for all the investigated inlet concentration and flow velocity.

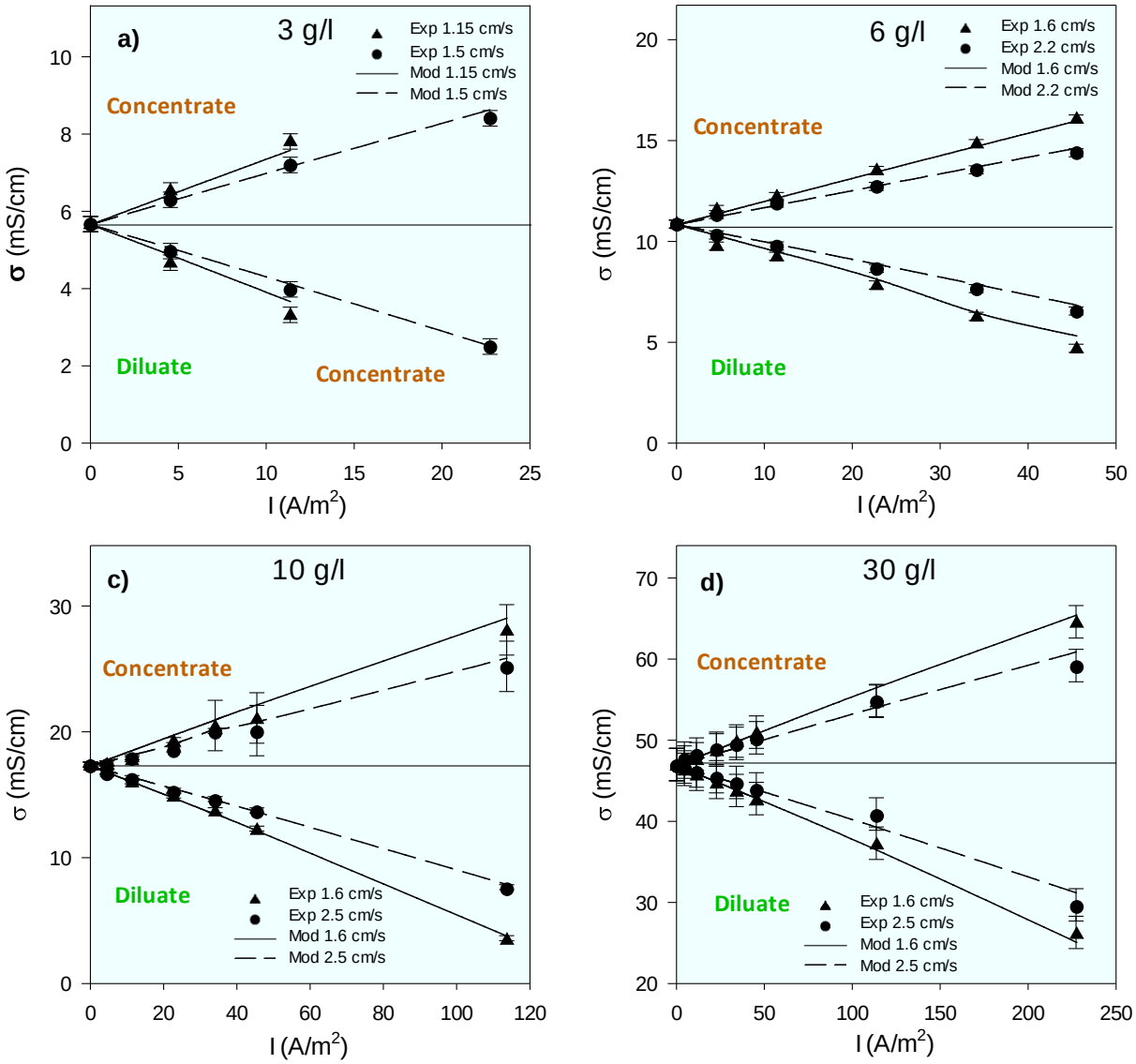


*Figure 4. Comparison between model predictions (lines) and experimental data (symbols), for both concentrate and diluate outlet conductivity at different currents, velocities, and feed concentrations: a) 3 g/l, b) 6 g/l, c) 10 g/l, d) 30 g/l. Stack area:10×79 cm², spacer thickness: 270 μm.*

A comprehensive overview on the model prediction accuracy for all experiments performed is reported in Figure 5, showing the parity plot for streams conductivity, i.e. the experimental outlet conductivity versus the conductivity calculated by the model for diluate and concentrate. Again, the model reliability is confirmed as most of the points are very close to the reference line $y = x$.

On this basis, it is worth noting that, compared to other literature works, the developed model has been validated in a much wider range of feed concentration (i.e., ranging from brackish water to seawater conditions), and is therefore suitable for a variety of possible applications. In the following sections, two examples of application of the model predictive capability to complex operating schemes are reported.

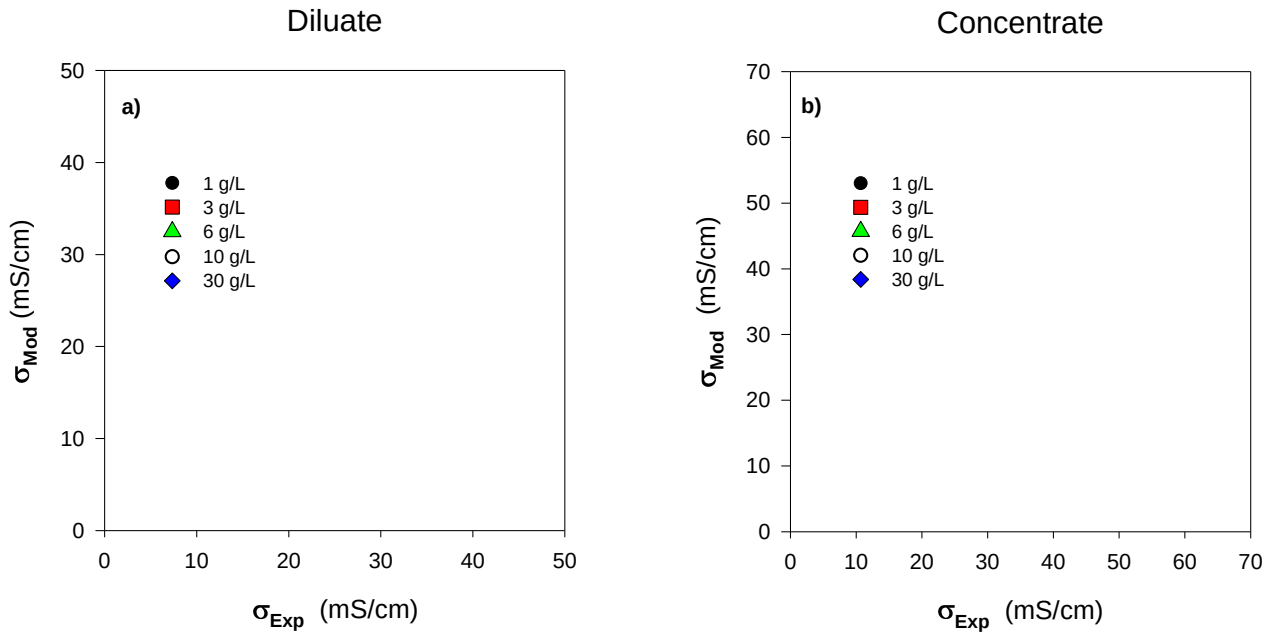


*Figure 5. Predicted vs. experimental outlet conductivities for a) diluate and b) concentrate for all performed experiments (symbols). Stack area:10×79 cm$^2$, spacer thickness: 270μm.*

## 5.2 Case I: Seawater multistage desalination

The model has been used to simulate a multistage ED system for seawater desalination, as this is a relatively newly explored application [24]. In fact, electrodialysis is not used nowadays for seawater desalination, mainly due to the high energy consumption compared to state-of-the-art desalination processes (e.g. reverse osmosis). However, the use of staging in ED is of importance, as this could lead to a reduction of the overall energy consumption. In this regard, the developed model has been used to assess the effect of different current/voltage distributions on the specific energy consumption, simulating a series of 4 ED stacks with fixed geometrical properties (active area, number of cell pairs,

spacer type), and arranged in co-current mode (Figure 8a). Table 3 summarises the process conditions and geometric parameters simulated for the 4-stage ED system.

*Table 3. Simulated geometric parameters and process conditions of a 4-stage ED system for seawater desalination. The flowrate refers to both the diluate and the concentrate separately. The co-current configuration is simulated and Fujifilm membranes are considered.*

| **Channel length** **L (cm)** | **Channel width** **b (cm)** | **Number of cell pairs** $N_{cp}$ | **Spacer thickness** $\delta_{SOL}$ **(μm)** | **Inlet velocity** **u (cm/s)** | **Inlet concentration** $C_{SOL}^{IN}$ **(mol/m$^3$)** | **Diluate outlet concentration** $C_D^{OUT}$ **(mol/m$^3$)** |
|---|---|---|---|---|---|---|
| 43 | 10 | 500 | 155 | 1.5 | 500 | 8.5 |

The model has been used to evaluate the effect of staging to desalinate seawater (500 mol/m$^3$ NaCl, i.e. ~30 g/l) to drinking water (500 ppm NaCl, i.e., ~8.5 mol/m$^3$ NaCl). In particular, two benchmark scenarios have been simulated: in the first scenario (i.e., "equal voltage"), the target diluate concentration is reached by applying the same voltage to the 4 stacks (i.e., 0.23 V per cell pair). Notably, this scenario corresponds to the case of a single stack with a flow path length equal to the sum of all stack lengths, and it can be considered as a reference case in the assessment of multistage operations. The second scenario ("equal current") accounts for the effect of multiple stages operating under the same overall current (2.43 A), in order to reach the target diluate concentration.

Figure 6 shows the main model results for a single cell pair along the length of the 4 stages, for both the "equal voltage" and the "equal current" cases. In particular, Figure 6 shows the cell pair voltage (Figure 6 A), current density and current efficiency (Figure 6 B), concentrations (Figure 6 C), flow rate distribution and apparent flux (Figure 6 D). Both the spatial distribution of current density (Figure 6 B) and the concentration (Figure 6 C) clearly show how the "equal voltage" case is highly inefficient compared to the "equal current" case. In the "equal voltage" scenario most of the desalination takes place in the first stage, leading to a poor ion removal in the following stages. As a consequence, the system is subjected to a large concentration difference over the membranes along most of the flow path length (i.e., after the first stage), thus causing larger water flux and salt back diffusion through the membranes, resulting in very low current efficiencies (Figure 6 B). The negative effect of water

transport can be seen from the decreasing concentration of the concentrate stream (Figure 6 C), as well as from the reduced diluate flowrate (Figure 6 D).

The "equal current" scenario, instead, shows a more homogenous ion removal along the four stacks, leading to lower water transport and higher current efficiency (Figure 6 B), which decreases significantly only in the last stage, especially close to the outlet. Figure 6 B clearly shows the benefits of staging with different voltage values ("equal current") to enhance the overall current efficiency, resulting in a significant reduction of the total specific energy consumption (i.e., 1.94 kWh/$m^3$ of product instead of 4.59 kWh/$m^3$ required by the "equal voltage" scenario).

These results also highlight that the large concentration difference arising between diluate and concentrate is one of the main issues for desalination of concentrated streams (i.e. seawater). It is worth noting that this preliminary analysis did not include other possible scenarios, such as the use of different current, stack geometry, or membranes per stage. All of these options need to be taken into account to properly optimise a multistage system.

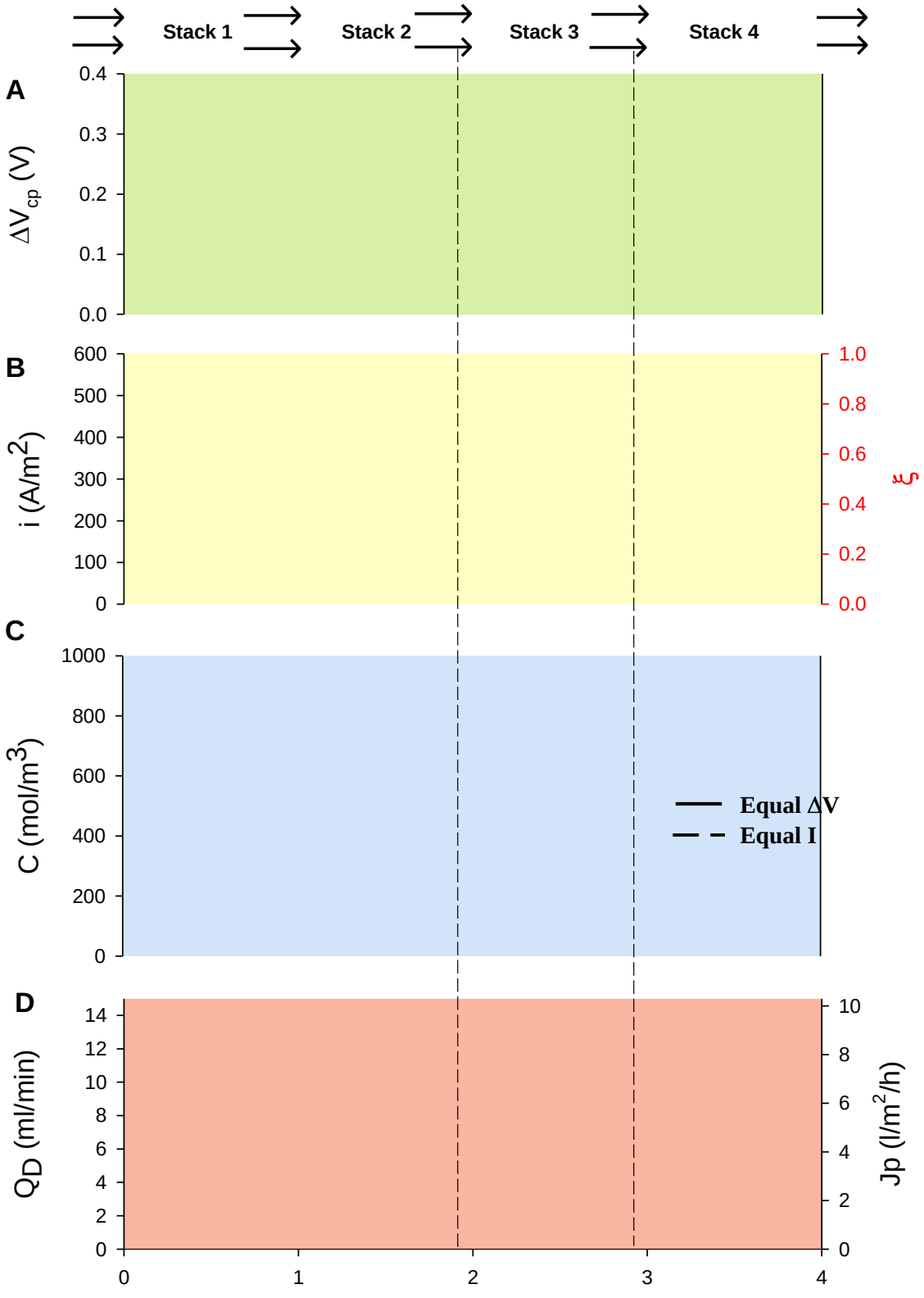


*Figure 6. Model predictions for a 4-stage 10×43 cm² ED co-current system equipped with 155 µm woven spacer, Fujifilm membranes and 500 cell pairs with 5.5 l/min flowrate. Solid lines: same voltage per stage (0.23 V per cell pair). Dashed lines: same current per stage (2.43 A). A: cell pair voltage, B: current density distribution (main axis) and local current efficiency (secondary axis), C: diluate and concentrate concentration, D: flowrate (main axis) and apparent product flux per single channel (secondary axis).*

### 5.3 Case II: Brackish water batch desalination

Another representative system simulated in this work is the batch ED operation for brackish water desalination (i.e., $C_{SOL}^{IN}$=5 g/l). In particular, a small lab scale unit has been simulated adopting the time-dependent formulation of the hierarchical model (see section 3.3.2). Stack features and operating conditions are reported in Table 4.

*Table 4. Geometric parameters of the ED unit equipped with Fujifilm membranes simulated in batch operation.*

| Channel length L (cm) | Channel width b (cm) | Number of cell pairs $N_{cp}$ | Spacer thickness $\delta_{SOL}$ (μm) | Inlet velocity u (cm/s) | Inlet concentration $C_{SOL}^{IN}$ (g/l) | Diluate outlet concentration $C_D^{OUT}$(g/l) |
|---|---|---|---|---|---|---|
| 10 | 10 | 10 | 270 | 2 | 5 | 0.25 |

Fixed voltage simulations have been performed (i.e. 3, 5 or 8 V, neglecting the voltage drop at the electrodes, $R_{blank}$) by assuming a 2 cm/s inlet flow velocity inside each channel. Then, the solution inside the diluate tank (initially filled with a volume of 0.5 l, as for the concentrate) has been processed until its concentration reaches 250 ppm, thus accounting for a safety margin on the outlet concentration compared to the standard 500 ppm.

In Figure 7, the predicted trends of concentrations, volumes in the tanks, current and current efficiency for the three different applied voltages are reported. As expected, increasing the applied voltage reduces the time to reach the target concentration (~ 40% reduction from 3 to 8 V) as for each single pass a higher amount of salt is removed (i.e. the distance between the dashed and the continuous line is largest at the highest voltage). Reducing the operation time (i.e., the number of the recirculation cycles of the solution through the stack) decreases the impact of water transport and salt back diffusion in the system. As a result, the overall current efficiency is slightly higher at 8 V, so that ~4% less current is required to reach the target concentration compared to the 3 V case. Despite this, the overall energy consumption increases from 1 kWh/m$^3$ (at the minimum voltage) up to 3.6 kWh/m$^3$ (at the maximum voltage value). Therefore, it is clear how the voltage increase has some beneficial effects such as higher current efficiency and lower desalination times, although, from an energetic

perspective, those advantages are overcome by the increase of the ohmic and non-ohmic energy dissipation, which result in a larger overall energy consumption. The competition of transport and energetic (voltage drop) phenomena suggests that, as well as for the multistage system, the batch process is particularly suitable for process optimisation. In particular, it is possible to design an optimal process where voltage (or current) changes through time, mimicking the effect of staging in time rather than in space.

Finally, it is worth noting that, in principle, a batch operation exhibits a lower energy efficiency compared to an equivalent single pass continuous operation, due to the effect of the tanks where the dilute stream exiting from the stack is concentrated again. However, the batch operation can still be considered advantageous for specific lab experiments, in small scale productions or when an accurate control of the desalination steps is required (e.g. to minimise limiting current issues).

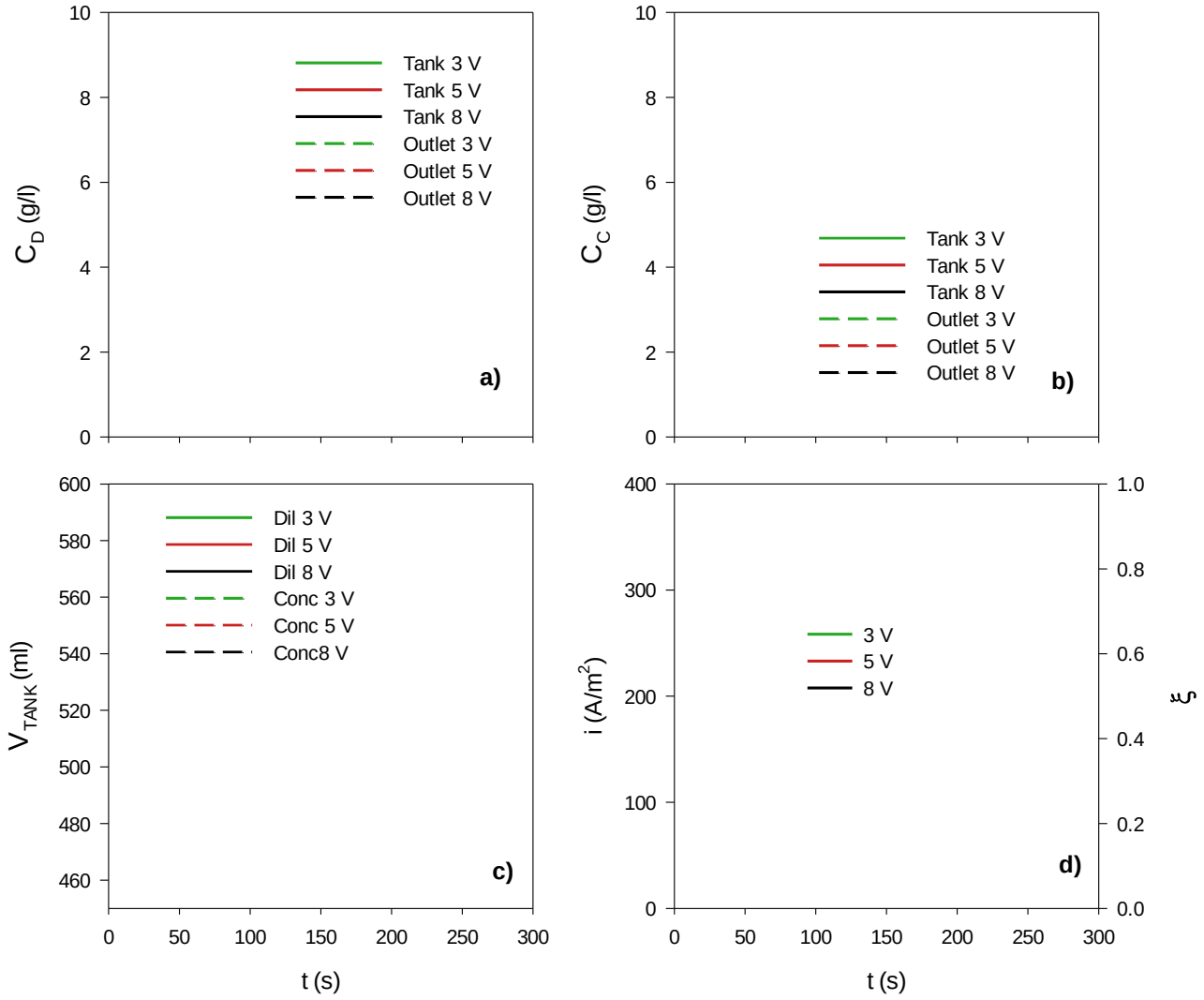


*Figure 7. Results as a function of time of batch ED simulations at different applied voltage. a) Diluate and b) concentrate concentration inside the tanks and at the stack outlet. c) Diluate and concentrate volumes in the tanks, d) Current density and current efficiency. 10×10 cm² stack with 270 μm spacers, 10 cell pairs (Fujifilm membranes) and 2 cm/s inlet flow velocity.*

## 6. Conclusions

A novel electrodialysis hierarchical model is presented for both brackish water and seawater desalination. The model was validated by comparison with original experimental data showing a good agreement with experiments in a wide range of inlet concentrations, from brackish water to seawater applications.

The main advantage of the hierarchical structure is the possibility to simulate complex schemes and operational strategies, allowing for higher flexibility and a wider applicability of the simulation tool.

In particular, two representative examples have been presented, i.e., i) seawater multistage desalination, and ii) brackish water batch desalination.

For the case of seawater multistage desalination, we have shown how the energy consumption could be drastically reduced by segmenting the operation, reducing the energy consumption from 4.59 kWh/m$^3$ to 1.94 kWh/m$^3$ only by changing the current distribution. Regarding the second example (brackish water batch desalination), we have simulated the dynamic operation of a batch ED desalination unit. This has shown how to identify an optimal trade-off between desalination time and energy consumption and paving the way for the optimisation of the applied-voltage on a time-scale, similarly to what was shown for the multistage ED on the space-scale.

**Acknowledgements**

This work has been performed within the REvivED water project (Low energy solutions for drinking water production by a REvival of ElectroDialysis systems). The REvivED water project has received funding from the European Union's Horizon 2020 research and innovation programme under Grant Agreement no. 685579 (www.revivedwater.eu).

The authors are grateful also to Deukum GmbH for supplying the ED stack adopted in the experimental set-up, FUJIFILM Manufacturing Europe for the membranes tested and Mr. Sergio La Manno for his contribution to the experimental campaign.

**List of symbols**

| | |
|---|---|
| $A$ | Membrane area (m$^2$) |
| $b$ | Membrane width (m) |
| $C$ | Concentration (mol/m$^3$) |
| $D$ | Diffusion coefficient (m$^2$/s) |
| $D^{IEM}$ | Salt permeability coefficient (m$^2$/s) |
| $d^{eq}$ | Equivalent diameter (m) |

| | |
|---|---|
| $E_{spec}$ | Specific energy consumption (J/m$^3$) |
| $E_{spec}^{salt}$ | Salt-specific energy consumption (J/mol) |
| $F$ | Faraday's constant (C/mol) |
| $f$ | Friction factor |
| $f_S$ | Shadow factor |
| $I$ | Current (A) |
| $i$ | Current density (A/m$^2$) |
| $J$ | Flux (mol/m$^2$/s) |
| $J_P$ | Apparent product flux (l/m$^2$/h) |
| $L$ | Channel length (m) |
| $L_p$ | Water permeability (m$^3$/Pa/s/m$^2$) |
| $N_{cp}$ | Number of cell pairs in a stack |
| $N_s$ | Number of stages |
| $P$ | Power consumption (W) |
| $\Delta p$ | Pressure drop (Pa) |
| $Q$ | Volumetric flow rate (m$^3$/s) |
| $q$ | Volumetric flux (m$^3$/m$^2$/s) |
| $R_G$ | Universal gas constant (J/mol/K) |
| $R$ | Areal electrical resistance (Ωm$^2$) |
| $Re$ | Reynolds number |
| $Sh$ | Sherwood number |
| $t^{co}$ | Co-ion transport number |
| $t^{counter}$ | Counter-ion transport number |
| $t$ | Time (s) |
| $u$ | Velocity (m/s) |
| $V$ | Volume (m$^3$) |
| $V_{tot}$ | Overall voltage drop (V) |
| $\Delta V_{cp}$ | Voltage drop over a cell pair (V) |
| $w$ | Total water transport number |
| $x$ | Coordinate in the direction of the main flow (m) |

**Greek letters**

| | |
|---|---|
| $\alpha$ | Permselectivity |
| $\gamma$ | Activity coefficient |
| $\delta$ | Channel or membrane thickness (m) |
| $\eta$ | Non-ohmic voltage drop (V) |
| $\nu$ | Van't Hoff coefficient |
| $\xi$ | Current efficiency |
| $\Lambda$ | Equivalent conductivity ($Sm^2/mol$) |
| $\pi$ | Osmotic pressure (Pa) |
| $\rho$ | Density ($kg/m^3$) |
| $\varphi$ | Osmotic coefficient |

**Subscripts and superscripts**

| | |
|---|---|
| $AEM$ | Anion-exchange membrane |
| $av$ | Average |
| $blank$ | Blank |
| $C$ | Concentrate |
| $CEM$ | Cation-exchange membrane |
| $co$ | Co-ion |
| $cond$ | Conductive |
| $counter$ | Counter-ion |
| $D$ | Dilute |
| $diff$ | Diffusive |
| $eosm$ | Electroosmotic |
| $i$ | Species *i* (cation or anion) |
| $IN$ | Inlet |
| $IEM$ | Ion-exchange membrane (anion, *AEM*, or cation, *CEM*) |
| $int$ | Solution-membrane interface |
| $ion$ | Ion |
| $osm$ | Osmotic |
| $OUT$ | Outlet |
| $SOL$ | Solution (dilute, *D*, or concentrate, *C*) |
| $tot$ | Total |
| $tank$ | Tank |

| | |
|---|---|
| *w* | Water |

## References


[1] W. (United N.W.W.A. Programme), The United Nations World Water Development Report 2017. Wastewater: The Untapped Resource, Paris.UNESCO, 2017.

[2] A. Subramani, J.G. Jacangelo, Emerging desalination technologies for water treatment: A critical review, Water Res. 75 (2015) 164–187. doi:10.1016/j.watres.2015.02.032.

[3] IDA, Desalination YearBook 2016-2017, Water Desalination Report, 2017.

[4] M. Nair, D. Kumar, Water desalination and challenges: The Middle East perspective: a review, Desalin. Water Treat. 51 (2013) 2030–2040. doi:10.1080/19443994.2013.734483.

[5] N. Ghaffour, T.M. Missimer, G.L. Amy, Technical review and evaluation of the economics of water desalination: Current and future challenges for better water supply sustainability, Desalination. 309 (2013) 197–207. doi:10.1016/j.desal.2012.10.015.

[6] H. Strathmann, Electrodialysis, a mature technology with a multitude of new applications, Desalination. 264 (2010) 268–288. doi:10.1016/j.desal.2010.04.069.

[7] A. Campione, L. Gurreri, M. Ciofalo, G. Micale, A. Tamburini, A. Cipollina, Electrodialysis for water desalination: A critical assessment of recent developments on process fundamentals, models and applications, Desalination. 434 (2018) 121–160. doi:10.1016/j.desal.2017.12.044.

[8] C. Larchet, V.I. Zabolotsky, N. Pismenskaya, V. V Nikonenko, A. Tskhay, K. Tastanov, G. Pourcelly, Comparison of different ED stack conceptions when applied for drinking water production from brackish waters, Desalination. 222 (2008) 489–496. doi:10.1016/j.desal.2007.02.067.

[9] M. Fidaleo, M. Moresi, Electrodialysis Applications in The Food Industry, Adv. Food Nutr. Res. 51 (2006) 265–360. doi:10.1016/S1043-4526(06)51005-8.

[10] F. Gonçalves, C. Fernandes, P. Cameira dos Santos, M.N. de Pinho, Wine tartaric stabilization by electrodialysis and its assessment by the saturation temperature, J. Food Eng. 59 (2003) 229–235. doi:10.1016/S0260-8774(02)00462-4.

[11] E. Vera, J. Ruales, M. Dornier, J. Sandeaux, R. Sandeaux, G. Pourcelly, Deacidification of clarified passion fruit juice using different configurations of electrodialysis, J. Chem. Technol. Biotechnol. 78 (2003) 918–925. doi:10.1002/jctb.827.

[12] C. Huang, T. Xu, Y. Zhang, Y. Xue, G. Chen, Application of electrodialysis to the production of organic acids: State-of-the-art and recent developments, J. Memb. Sci. 288 (2007) 1–12. doi:10.1016/j.memsci.2006.11.026.

[13] F. Fu, Q. Wang, Removal of heavy metal ions from wastewaters: A review, J. Environ. Manage. 92 (2011) 407–418. doi:10.1016/j.jenvman.2010.11.011.

[14] L. Marder, A.M. Bernardes, J. Zoppas Ferreira, Cadmium electroplating wastewater treatment using a laboratory-scale electrodialysis system, Sep. Purif. Technol. 37 (2004) 247–255. doi:10.1016/j.seppur.2003.10.011.

[15] M.A. Acheampong, R.J.W. Meulepas, P.N.L. Lens, Removal of heavy metals and cyanide from gold mine wastewater, J. Chem. Technol. Biotechnol. 85 (2010) 590–613. doi:10.1002/jctb.2358.

[16] T. Yamabe, Present status of electrodialysis in Japan, Desalination. 23 (1977) 195–202. doi:10.1016/S0011-9164(00)82522-9.

[17] A. Al-Karaghouli, L.L. Kazmerski, Energy consumption and water production cost of conventional and renewable-energy-powered desalination processes, Renew. Sustain. Energy Rev. 24 (2013) 343–356. doi:10.1016/j.rser.2012.12.064.

[18] F. Valero, R. Arbós, Desalination of brackish river water using Electrodialysis Reversal (EDR): Control of the THMs formation in the Barcelona (NE Spain) area, Desalination. 253 (2010) 170–174. doi:10.1016/j.desal.2009.11.011.

[19] C. Hanrahan, L. Karimi, A. Ghassemi, A. Sharbat, High-recovery electrodialysis reversal for the desalination of inland brackish waters, Desalin. Water Treat. 57 (2016) 11029–11039. doi:10.1080/19443994.2015.1041162.

[20] A.M. Lopez, M. Williams, M. Paiva, D. Demydov, T.D. Do, J.L. Fairey, Y.P.J. Lin, J.A. Hestekin, Potential of electrodialytic techniques in brackish desalination and recovery of industrial process water for reuse, Desalination. 409 (2017) 108–114. doi:10.1016/j.desal.2017.01.010.

[21] V.A. Shaposhnik, K. Kesore, An early history of electrodialysis with permselective membranes, J. Memb. Sci. 136 (1997) 35–39. doi:10.1016/S0376-7388(97)00149-X.

[22] V.D. Grebenyuk, O. V. Grebenyuk, Electrodialysis: From an idea to realization, Russ. J. Electrochem. 38 (2002) 806–809. doi:10.1023/A:1016897224948.

[23] J. Ran, L. Wu, Y. He, Z. Yang, Y. Wang, C. Jiang, L. Ge, E. Bakangura, T. Xu, Ion exchange membranes: New developments and applications, J. Memb. Sci. 522 (2017) 267–291.

[24] E.U., REvivED water, (2016).

[25] M.R. Adiga, S.K. Adhikary, P.K. Narayanan, W.P. Harkare, S.D. Gomkale, K.P. Govindan, Performance analysis of photovoltaic electrodialysis desalination plant at Tanote in Thar desert, Desalination. 67 (1987) 59–66. doi:10.1016/0011-9164(87)90232-3.

[26] J.M. Veza, B. Penate, F. Castellano, Electrodialysis desalination designed for off-grid wind energy, Desalination. 160 (2004) 211–221. doi:10.1016/S0011-9164(04)90024-0.

[27] M. Vanoppen, G. Blandin, S. Derese, P. Le Clech, J. Post, A.R.D. Verliefde, Salinity gradient power and desalination, in: Sustain. Energy from Salin. Gradients, Elsevier, 2016: pp. 281–313. doi:10.1016/B978-0-08-100312-1.00009-2.

[28] Q. Wang, X. Gao, Y. Zhang, Z. He, Z. Ji, X. Wang, C. Gao, Hybrid RED/ED system: Simultaneous osmotic energy recovery and desalination of high-salinity wastewater, Desalination. 405 (2017) 59–67. doi:10.1016/j.desal.2016.12.005.

[29] H.J. Lee, F. Sarfert, H. Strathmann, S.H. Moon, Designing of an electrodialysis desalination plant, Desalination. 142 (2002) 267–286. doi:10.1016/S0011-9164(02)00208-4.

[30] M. Sadrzadeh, A. Kaviani, T. Mohammadi, Mathematical modeling of desalination by electrodialysis, Desalination. 206 (2007) 538–546. doi:10.1016/j.desal.2006.04.062.

[31] Z. Zourmand, F. Faridirad, N. Kasiri, T. Mohammadi, Mass transfer modeling of desalination through an electrodialysis cell, Desalination. 359 (2015) 41–51. doi:10.1016/j.desal.2014.12.008.

[32] K. Tado, F. Sakai, Y. Sano, A. Nakayama, An analysis on ion transport process in electrodialysis desalination, Desalination. 378 (2016) 60–66. doi:10.1016/j.desal.2015.10.001.

[33] R. Enciso, J.A. Delgadillo, O. Domínguez, I. Rodríguez-Torres, Analysis and validation of the hydrodynamics of an electrodialysis cell using computational fluid dynamics, Desalination. 408 (2017) 127–132. doi:10.1016/j.desal.2017.01.015.

[34] M. Tedesco, H.V.M. Hamelers, P.M. Biesheuvel, Nernst-Planck transport theory for (reverse) electrodialysis: I. Effect of co-ion transport through the membranes, J. Memb. Sci. 510 (2016) 370–381.

[35] M. Tedesco, H.V.M. Hamelers, P.M. Biesheuvel, Nernst-Planck transport theory for (reverse) electrodialysis: II. Effect of water transport through ion-exchange membranes, J. Memb. Sci. 531 (2017) 172–182. doi:10.1016/j.memsci.2017.02.031.

[36] Y. Tanaka, Concentration polarization in ion-exchange membrane electrodialysis: The events arising in an unforced flowing solution in a desalting cell, J. Memb. Sci. 244 (2004) 1–16. doi:10.1016/j.memsci.2004.02.041.

[37] L. Gurreri, G. Battaglia, A. Tamburini, A. Cipollina, G. Micale, M. Ciofalo, Multi-physical modelling of reverse electrodialysis, Desalination. 423 (2017) 52–64. doi:10.1016/j.desal.2017.09.006.

[38] P.N. Pintauro, D.N. Bennion, Mass transport of electrolytes in membranes. 1. Development of mathematical transport model, Ind. Eng. Chem. Fundam. 23 (1984) 230–234.

[39] G. Kraaijeveld, V. Sumberova, S. Kuindersma, H. Wesselingh, Modelling electrodialysis using the Maxwell-Stefan description, Chem. Eng. J. Biochem. Eng. J. 57 (1995) 163–176. doi:10.1016/0923-0467(94)02940-7.

[40] J.A. Wesselingh, P. Vonk, G. Kraaijeveld, Exploring the Maxwell-Stefan description of ion exchange, Chem. Eng. J. Biochem. Eng. J. 57 (1995) 75–89. doi:10.1016/0923-0467(94)02932-6.

[41] K.M. Chehayeb, J.H. Lienhard, Entropy generation analysis of electrodialysis, Desalination. 413 (2017) 184–198. doi:10.1016/j.desal.2017.03.001.

[42] M. Fidaleo, M. Moresi, Optimal strategy to model the electrodialytic recovery of a strong electrolyte, J. Memb.

Sci. 260 (2005) 90–111. doi:10.1016/j.memsci.2005.01.048.

[43] R.K. McGovern, S.M. Zubair, J.H. Lienhard V, The cost effectiveness of electrodialysis for diverse salinity applications, Desalination. 348 (2014) 57–65. doi:10.1016/j.desal.2014.06.010.

[44] J.M. Ortiz, J.A. Sotoca, E. Expósito, F. Gallud, V. García-García, V. Montiel, A. Aldaz, Brackish water desalination by electrodialysis: Batch recirculation operation modeling, J. Memb. Sci. 252 (2005) 65–75. doi:10.1016/j.memsci.2004.11.021.

[45] P. Tsiakis, L.G. Papageorgiou, Optimal design of an electrodialysis brackish water desalination plant, Desalination. 173 (2005) 173–186. doi:10.1016/j.desal.2004.08.031.

[46] N.A.A. Qasem, B.A. Qureshi, S.M. Zubair, Improvement in design of electrodialysis desalination plants by considering the Donnan potential, Desalination. 441 (2018) 62–76. doi:10.1016/j.desal.2018.04.023.

[47] B.A. Qureshi, S.M. Zubair, Design of electrodialysis desalination plants by considering dimensionless groups and variable equivalent conductivity, Desalination. 430 (2018) 197–207. doi:10.1016/j.desal.2017.12.030.

[48] R.K. McGovern, A.M. Weiner, L. Sun, C.G. Chambers, S.M. Zubair, J.H. Lienhard V, On the cost of electrodialysis for the desalination of high salinity feeds, Appl. Energy. 136 (2014) 649–661. doi:10.1016/j.apenergy.2014.09.050.

[49] K.M. Chehayeb, D.M. Farhat, K.G. Nayar, J.H. Lienhard, Optimal design and operation of electrodialysis for brackish-water desalination and for high-salinity brine concentration, Desalination. 420 (2017) 167–182. doi:10.1016/j.desal.2017.07.003.

[50] M. La Cerva, M. Di Liberto, L. Gurreri, A. Tamburini, A. Cipollina, G. Micale, M. Ciofalo, Coupling CFD with simplified 1-D models to predict the performance of reverse electrodialysis stacks, J. Memb. Sci. 541 (2017) 595–610. doi:10.1016/j.memsci.2017.07.030.

[51] M. Tedesco, A. Cipollina, A. Tamburini, I.D.L. Bogle, G. Micale, A simulation tool for analysis and design of reverse electrodialysis using concentrated brines, Chem. Eng. Res. Des. 93 (2015) 441–456. doi:10.1016/j.cherd.2014.05.009.

[52] A.M. Weiner, R.K. McGovern, J.H. Lienhard V, Increasing the power density and reducing the levelized cost of electricity of a reverse electrodialysis stack through blending, Desalination. 369 (2015) 140–148. doi:10.1016/j.desal.2015.04.031.

[53] K.M. Chehayeb, K.G. Nayar, J.H. Lienhard, On the merits of using multi-stage and counterflow electrodialysis for reduced energy consumption, Desalination. 439 (2018) 1–16. doi:10.1016/j.desal.2018.03.026.

[54] S. Pawlowski, V. Geraldes, J.G. Crespo, S. Velizarov, Computational fluid dynamics (CFD) assisted analysis of profiled membranes performance in reverse electrodialysis, J. Memb. Sci. 502 (2016) 179–190.

[55] N.C. Wright, S.R. Shah, S.E. Amrose, A.G. Winter, A robust model of brackish water electrodialysis desalination with experimental comparison at different size scales, Desalination. 443 (2018) 27–43. doi:10.1016/J.DESAL.2018.04.018.

[56] M. La Cerva, L. Gurreri, M. Tedesco, A. Cipollina, M. Ciofalo, A. Tamburini, G. Micale, Determination of limiting current density and current efficiency in electrodialysis units, Desalination. 445 (2018) 138–148. doi:10.1016/J.DESAL.2018.07.028.

[57] S.R. Shah, N.C. Wright, P.A. Nepsky, A.G. Winter, Cost-optimal design of a batch electrodialysis system for domestic desalination of brackish groundwater, Desalination. 443 (2018) 198–211. doi:10.1016/j.desal.2018.05.010.

[58] K.S. Pitzer, Thermodynamics of electrolytes. I. Theoretical basis and general equations, J. Phys. Chem. 77 (1973) 268–277. doi:10.1021/j100621a026.

[59] C.F. Weber, Calculation of Pitzer Parameters at High Ionic Strengths, Ind. Eng. Chem. Res. 39 (2000) 4422–4426. doi:10.1021/ie000411o.

[60] J.R. Wilson, Demineralization by electrodialysis, Butterworths Scientific Publications, 1960.

[61] A. Despić, G.J. Hills, Electro-osmosis in charged membranes. The determination of primary solvation numbers, Discuss. Faraday Soc. 21 (1956) 150. doi:10.1039/df9562100150.

[62] S.S. Islam, R.L. Gupta, K. Ismail, Extension of the Falkenhagen-Leist-Kelbg equation to the electrical conductance of concentrated aqueous electrolytes, J. Chem. Eng. Data. 36 (1991) 102–104. doi:10.1021/je00001a031.

[63] V. V Wagholikar, H. Zhuang, Y. Jiao, N.E. Moe, H. Ramanan, L.M. Goh, J. Barber, K.S. Lee, H.P. Lee, J.Y.H. Fuh, Modeling cell pair resistance and spacer shadow factors in electro-separation processes, J. Memb. Sci. 543 (2017) 151–162. doi:10.1016/J.MEMSCI.2017.08.054.

[64] J. Veerman, M. Saakes, S.J. Metz, G.J. Harmsen, Reverse electrodialysis: Performance of a stack with 50 cells on the mixing of sea and river water, J. Memb. Sci. 327 (2009) 136–144. doi:10.1016/j.memsci.2008.11.015.

[65] S. Mehdizadeh, M. Yasukawa, T. Abo, Y. Kakihana, M. Higa, Effect of spacer geometry on membrane and solution compartment resistances in reverse electrodialysis, J. Memb. Sci. 572 (2019) 271–280. doi:10.1016/J.MEMSCI.2018.09.051.

[66] A.H. Galama, N.A. Hoog, D.R. Yntema, Method for determining ion exchange membrane resistance for electrodialysis systems, Desalination. 380 (2016) 1–11. doi:10.1016/j.desal.2015.11.018.

[67] P. Długołęcki, P. Ogonowski, S.J. Metz, M. Saakes, K. Nijmeijer, M. Wessling, P. Długołecki, P. Ogonowski, S.J. Metz, M. Saakes, K. Nijmeijer, M. Wessling, On the resistances of membrane, diffusion boundary layer and double layer in ion exchange membrane transport, J. Memb. Sci. 349 (2010) 369–379. doi:10.1016/j.memsci.2009.11.069.

[68] S. Zhu, R.S. Kingsbury, D.F. Call, O. Coronell, Impact of solution composition on the resistance of ion exchange membranes, J. Memb. Sci. 554 (2018) 39–47. doi:10.1016/J.MEMSCI.2018.02.050.

[69] N. Lakshminarayanaiah, Transport phenomena in artificial membranes, Chem. Rev. 65 (1965) 491.

[70] K. Kontturi, L. Murtomäki, J.A. Manzanares, Ionic Transport Processes, Oxford University Press, New York, 2008. doi:10.1093/acprof:oso/9780199533817.001.0001.

[71] H. Strathmann, Ion-exchange membrane separation processes, First ed., Elsevier, Amsterdam, 2004.

[72] L. Gurreri, A. Tamburini, A. Cipollina, G. Micale, M. Ciofalo, CFD prediction of concentration polarization phenomena in spacer-filled channels for reverse electrodialysis, J. Memb. Sci. 468 (2014) 133–148. doi:10.1016/j.memsci.2014.05.058.

[73] L. Gurreri, A. Tamburini, A. Cipollina, G. Micale, M. Ciofalo, Flow and mass transfer in spacer-filled channels for reverse electrodialysis: a CFD parametrical study, J. Memb. Sci. 497 (2016) 300–317. doi:10.1016/j.memsci.2015.09.006.

[74] L. Gurreri, M. Ciofalo, A. Cipollina, A. Tamburini, W. Van Baak, G. Micale, CFD modelling of profiled-membrane channels for reverse electrodialysis, Desalin. Water Treat. 55 (2015) 1–20. doi:10.1080/19443994.2014.940651.

[75] L. Gurreri, A. Tamburini, A. Cipollina, G. Micale, M. Ciofalo, Pressure drop at low reynolds numbers in woven-spacer-filled channels for membrane processes: CFD prediction and experimental validation, Desalin. Water Treat. 61 (2017) 170–182. doi:10.5004/dwt.2016.11279.

**Appendix A: Transport numbers estimation**

The counter-ion transport number in the membrane ($t_{IEM}^{counter}$) can be directly linked with the membrane permselectivity using the following expression [71]:

$$\alpha_{IEM} = \frac{t_{IEM}^{counter} - t_{SOL}^{counter}}{t_{SOL}^{co}} \tag{24}$$

where $t^{counter}$ and $t^{co}$ are the transport number of the same counter-ion and co-ion in solution, and the subscript $IEM$ indicates that, using the relevant values, the expression is valid for both AEM and CEM.

It is worth noting that the term $[t_{CEM}^{counter} - (1 - t_{AEM}^{counter})]$ in eq. (1) is representative of the non-ideal permselectivity of the membranes, as it accounts for the conductive co-ion transport through IEMs that in practice results in a drop of the salt removal efficiency of the system.

**Appendix B: Pitzer's correlations for osmotic coefficients and activity coefficients**

In order to estimate osmotic coefficient ($\varphi$), the following Pitzer equation was adopted [58,59]:

$$\varphi - 1 = -A_1 \frac{\sqrt{m}}{1 + b'\sqrt{m}} + mB^{\varphi} + m^2 C^{\varphi} \tag{25}$$

$$B^{\varphi} = \beta^{(0)} + \beta^{(1)} e^{-\alpha\sqrt{m}} \tag{26}$$

where $A_1$ is the modified Debye-Huckel constant (0.3915 at 25 °C), $b'$is a correlation constant equal to 1.2, $m$ is the molality of the electrolyte, $\alpha$ is a fixed constant with a value of 2 (kg/mol)$^{1/2}$, $\beta^{(0)}$, $\beta^{(1)}$, $C^{\varphi}$are functions of the nature of the electrolyte and amount to 0.06743, 0.3301 and 0.00263, respectively, for NaCl.

Similarly, the Pitzer model can be used to estimate the average activity coefficient of salt in solution ($\gamma_{\pm}$) [58,59]:

$$ln\gamma_{\pm} = -A_1\left[\frac{\sqrt{m}}{1+b'\sqrt{m}} + \frac{2}{b'}\ln\left(1+b'\sqrt{m}\right)\right] + mB^{\gamma} + m^2C^{\gamma} \quad (27)$$

$$B^{\gamma} = 2\beta^{(0)} + 2\beta^{(1)}\left[1-\left(1+\alpha\, m^{\frac{1}{2}} - \frac{\alpha^2 m}{2}\right) exp\left(-\alpha\, m^{\frac{1}{2}}\right)\right]/\alpha^2 m \quad (28)$$

$$C^{\gamma} = \frac{3}{2}\, C^{\varphi} \quad (29)$$

**Appendix C: Islam's correlation for equivalent conductivity estimation**

The equivalent conductivity has been estimated through the correlation by Islam et al. [62]:

$$\Lambda(x) = \left[\Lambda^0 - \frac{B'_1(C)\sqrt{C}}{1+B'(C)\, a\sqrt{C}}\right]\left[1 - \frac{B'_2(C)\sqrt{C}}{1+B'(C)\, a\sqrt{C}}F'(C)\right] \quad (30)$$

$$B'(C) = 50.29 \cdot 10^8/(\varepsilon T)^{1/2} \quad (31)$$

$$B'_1(C) = 82.5/\left[\eta(\varepsilon T)^{1/2}\right] \quad (32)$$

$$B'_2(C) = 8.204 \cdot 10^5/(\varepsilon T)^{3/2} \quad (33)$$

$$F'(C) = \frac{\left[exp\left(0.2929\, B'\, C^{1/2}a\right) - 1\right]}{(0.2929\, B'\, cC^{1/2}a)} \quad (34)$$

where $\Lambda^0$ is the equivalent conductivity at infinite dilution, $C$ is the molar concentration, $\eta$ is the viscosity, $\varepsilon$ the dielectric constant and $T$ the electrolyte solution temperature and $a = 3.79\, A^o$ for NaCl. The main advantage of using this correlation is that it can reliably predict the conductivity even at high ionic strength (i.e. with concentrated brines).

**Appendix D: Dependence of membrane resistance on solution concentration**

According to the experimental data by Galama et al. [66], membrane resistance appears to be generally influenced by diluate solution concentration. Based on those findings, the following trend can be attributed to membrane resistance:

$$R_{IEM}(x) = R_{IEM}^{HIGH} + \frac{a}{C(x)^n} \tag{35}$$

where $R_{IEM}^{HIGH}$, $a$ and $n$ and are constants o value $7\times10^{-3}$ and 1.25 respectively. In this specific case, $R_{IEM}^{HIGH}$ has been taken equal to the value of the resistance measured at the standard concentration of 0.5 M NaCl (see Table 1). The values of the other constants are obtained by assuming the same trend of membrane resistance against the diluate concentration reported in Galama's work [66].

## Appendix E: Concentration polarisation and pressure drops

Neglecting the salt back-diffusion, eq. (2), the interface salt concentrations (solution side) appearing in eq. (13) can be estimated by the following relations [7,50]:

$$C_C^{int,IEM}(x) = C_C(x) + \frac{\left(t_{IEM}^{counter} - t^{ion}\right) i(x)}{F\, Sh_C^{IEM}(x)} \frac{d_C^{eq}}{D_C} \tag{36}$$

$$C_D^{int,IEM}(x) = C_D(x) - \frac{\left(t_{IEM}^{counter} - t^{ion}\right) i(x)}{F Sh_D^{IEM}(x)} \frac{d_D^{eq}}{D_D} \tag{37}$$

where $Sh$ is the Sherwood number, $D$ is the salt diffusion in solution and $d_{eq}$ is the equivalent diameter, here assumed equal to two times the channel thickness. Sherwood numbers, in turn, are computed through correlations obtained by 3-D CFD simulations for various spacer or profiled membrane geometries [72–74].

Pumping power is usually negligible compared to electric power consumed directly by the stack ($\Delta V\, I$), especially when high salinity feeds (e.g. seawater) are treated. However, it may play a significant role, depending on stack features and operating conditions. CFD correlations are also used in order to calculate the pressure drop distributed along the channels [75] and, thus, the pumping power consumption in eq. (15). In particular:

$$\Delta p_{SOL} = \frac{1}{2} f_{SOL} \frac{\rho_{SOL} {u_{SOL}^{av}}^2}{d_{SOL}^{eq}} L \tag{38}$$

where $\Delta p$ is the pressure drop, $\rho$ is the density of solution, $f$ is the Darcy friction coefficient that it is correlated to the Reynolds number [50,73] and $u^{av}$ is the average superficial velocity, with the local superficial velocity being defined as:

$$u_{SOL}(x) = \frac{Q_{SOL}(x)}{b\ \delta_{SOL}} \tag{39}$$

In the calculation of the total pressure drop, the hydraulic losses through the manifolds may be included using empirical data or, again, simulation results. It is worth noting that, as the stack geometrical features vary, the relevance of this contribution on the total pressure drop may change significantly [7].

## Appendix F: Overall plant schematics

This section shows some examples of process layouts that the model is able to simulate. The schemes can either include a single ED unit (i.e. batch process) or multiple stages (i.e. standard multistage ED and variations).

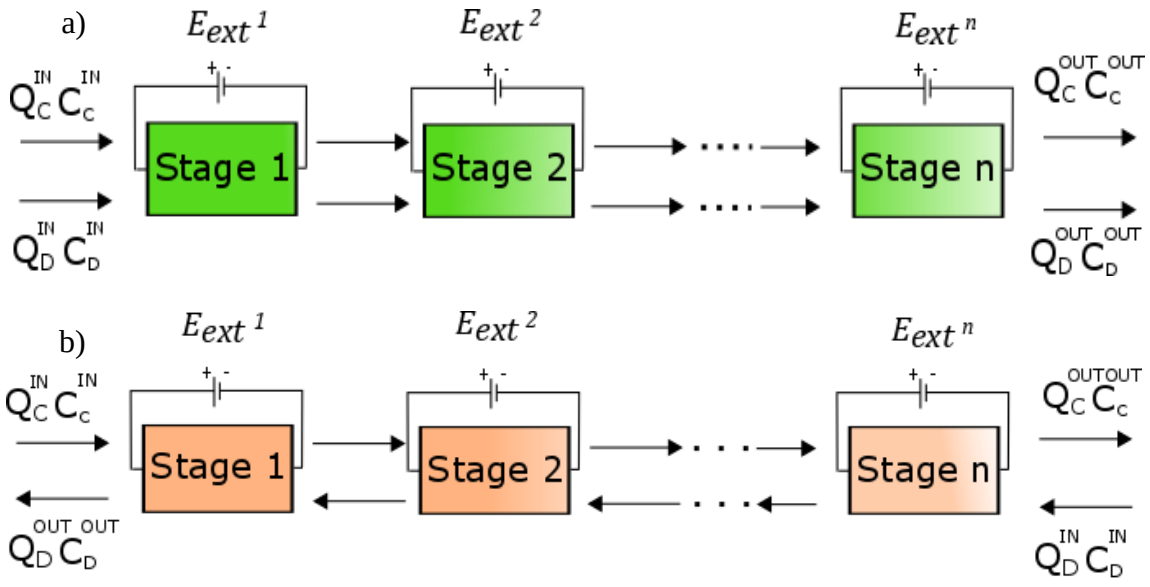


*Figure 8. Block diagrams of multistage ED processes in series in the case of a) co-current and b) counter-current arrangement.*

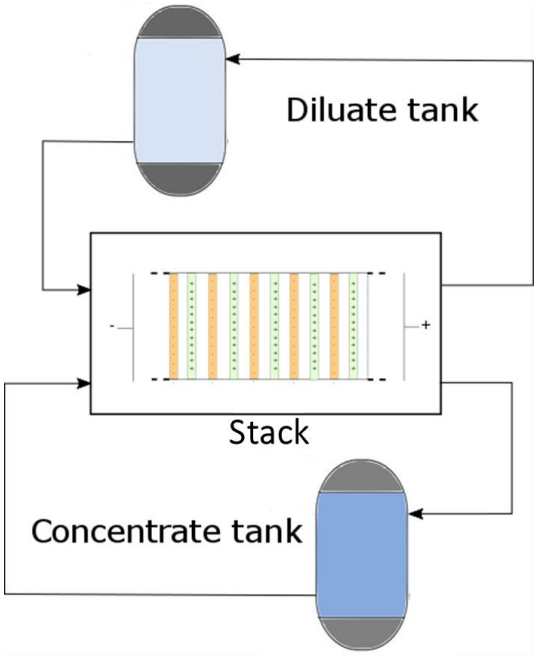


*Figure 9. Batch ED block scheme including the ED unit and the recirculation tanks.*

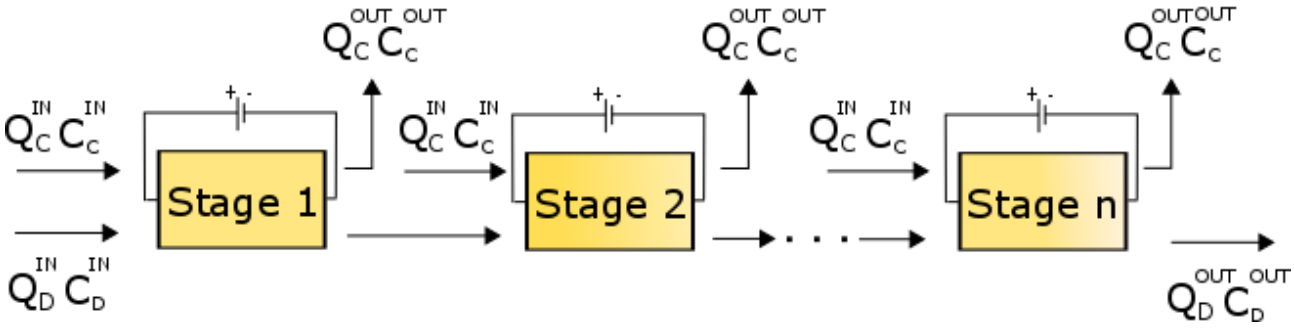


*Figure 10. Block scheme of a multistage system in which each stage has an independent feed. This kind of scheme can be useful in seawater desalination to reduce the concentration difference inside the stacks by feeding the concentrate compartments of each stage with fresh seawater.*

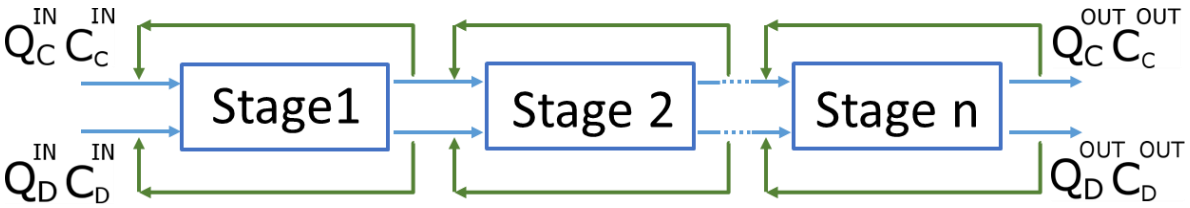


*Figure 11. Block scheme of a multistage system with concentrate and diluate feed & bleed. This kind of scheme is useful to either control the system recovery ratio by changing the amount of recycled solution or to increase the velocity inside the unit to reduce limiting current issues.*

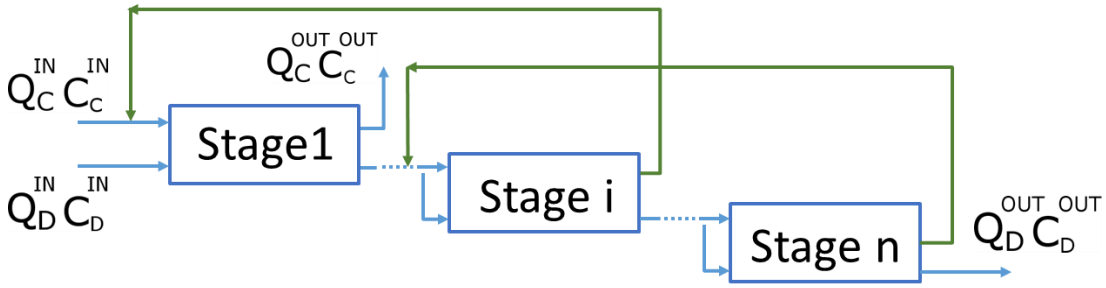


*Figure 12. Block scheme of a multistage system with interstage recycles. Each stage can recirculate its outlet concentrate back to the feed concentrate of one previous stage, while the diluate in each stage is fed to both concentrate and diluate compartments of the next stage. In this way, it is possible to control and reduce the concentration difference inside each unit.*